Controlling the Optical, Electrical and Chemical Properties of Carbon Inverse Opal by Nitrogen Doping

*Aarón Morelos-Gómez, Pierre G. Mani-González, Ali E. Aliev, Emilio Muñoz-Sandoval, Alberto Herrera-Gómez, Anvar A. Zakhidov, Humberto Terrones, Morinobu Endo, and Mauricio Terrones**

Nitrogen-doped carbon inverse opal (CIO-N) is synthesized by a two-step process involving the infiltration of carbon-nitrogen precursors within opals followed by the thermolysis and removal of the opal structure in hydrofluoric acid (HF). Undoped samples exhibit a reflection peak in the red region of the spectrum whereas N-doped samples display shifts to the blue region of the spectrum as the nitrogen content is increased. The degree of crystallinity of CIO-N strongly depends upon the nitrogen content and on the size of the precursor silica particles used to prepare the inverted opals. In addition, the introduction of nitrogen into the samples is able to increase the electrical conductivity by one order of magnitude from 2 to 30 S cm^{-1} (at room temperature). All samples are characterized by scanning electron microscopy (SEM), transmission electron microscopy (TEM), X-ray diffraction (XRD), Raman spectroscopy, X-ray photoelectron spectroscopy (XPS), ultraviolet-visible (UV-Vis) spectroscopy, and electrical conductivity measurements. It is envisaged that CIO-N could have important applications in the fabrication of photonic crystals, photoconducting materials, molecular sensors, field emission devices, capacitors, batteries, among many others.

1. Introduction

Porous carbon materials have been used as components in hydrogen storage cells, catalytic materials, filters, biosensors, capacitors and batteries.[1–7] It has been demonstrated that it is possible to modify the electronic, mechanical and chemical properties of carbon materials (CM) via doping: For example the introdution of foreign atoms within the carbon network. The most common elements able to dope CM are nitrogen and boron because of their similarities in size. Among various methods for doping porous carbon materials (PCM), we could mention: 1) reactions of porous carbon with gaseous sources containing nitrogen,[8] 2) co-carbonization of precursors containing carbon and nitrogen;[9] and 3) carbonization of materials containing nitrogen.[10] Other forms of CM include inverse opals, which consist of porous carbons obtained

Dr. A. Morelos-Gómez, Prof. E. Muñoz-Sandoval
Advanced Materials Department, IPICYT,
Camino a la Presa San José 2055, Col. Lomas 4a sección,
San Luis Potosí S.L.P., 78216, México
Dr. P. G. Mani-González, Prof. A. Herrera-Gómez
CINVESTAV-Querétaro, Libramiento Norponiente 2000,
Querétaro, 76230, México
Dr. P. G. Mani-González
Instituto de Ingeniería y Tecnología
Departamento de Física y Matemáticas
Universidad Autónoma de Ciudad Juárez
Ave. Del Charro 450, Cd. Juárez C.P. 32310, Chihuahua, México
Dr. A. Morelos-Gómez, Prof. A. E. Aliev, Prof. A. A. Zakhidov
The Alan G. MacDiarmid NanoTech Institute
University of Texas at Dallas
Richardson, TX, 75083, USA
Prof. H. Terrones
Department of Physics & Center for 2-Dimensional
and Layered Materials
The Pennsylvania State University
104 Davey Lab., University Park, PA, 16802–6300, USA
Dr. A. Morelos-Gómez, Prof. M. Endo
Institute for Carbon Science and Technology
Shinshu University
4–17–1 Wakasato, Nagano city, 380–8553, Japan
Prof. M. Endo, Prof. M. Terrones
Research Center for Exotic Nanocarbons (JST)
Shinshu University
Wakasato 4–17–1, Nagano, 380–8553, Japan
Prof. M. Terrones
Department of Physics
Department of Chemistry
Department of Materials Science and Engineering
and Materials Research Institute & Center for 2-Dimensional
and Layered Materials
The Pennsylvania State University
104 Davey Lab., University Park, PA, 16802–6300, USA
E-mail: mtterrones@shinshu-u.ac.jp, mut11@psu.edu

DOI: 10.1002/adfm.201303391

as a result of removing periodic arrays of silica spheres (opal) from carbon impregnated opals. The first synthesis of inverse opals, using silica particles as templates, was reported by Zakhidov et al. in 1998.[11] Other authors have used different types of carbon sources to impregnate the silica sphere array: sucrose, polyacrylnitrile, propylene, and others.[12–14] Depending on the chemical and structural nature of the carbon source used to impregnate opals, different types of pyrolized carbons could result after thermolysis.[15] For example, sucrose when heated up to 1000 °C generates a non-graphitizable carbon that does not transform into well ordered graphitic layers; the resulting structure mainly consists of tightly curled single carbon layers exhibiting Fullerene-like and Schwarzite-like structures.[16,17]

Porous photonic crystals are those materials exhibiting an ordered array of pores that interfere with photons, thus allowing certain wavelengths to propagate (or not) within the structure. It is possible to tune the optical properties of porous photonic crystals by swelling a polymeric inverse opal upon pH and ionic strength. Due to the change in volume, the diffraction wavelength also gets shifted.[18] Another way to tune the optical properties consists of introducing liquid crystals in the presence of an electric field.[19] In addition, there are many other methods that have been reviewed by Aguirre et al.[20] For carbon inverse opals, it was possible to alter the optical properties by doping with potassium.[21]

Introduction of nitrogen atoms within carbon materials could modify their optical properties by shifting its optical band gap.[22] For example, it has been observed that the insertion of nitrogen in amorphous carbon films could increase both the dielectric function and the refractive index.[23] However, there are examples in which the refractive index decreases with the introduction of nitrogen atoms.[24] Since nitrogen atom has one electron more when compared to carbon, nitrogen-doped carbon materials are expected to enhance significantly their chemical reactivity and also their electrical conductivity is increased due to the availability of additional electrons within the system.[25–29] Other advantages of nitrogen-doped carbon systems is the fact that they could be more biocompatible than their undoped counterparts and may be used as sensors or bio-markers.[30–33] In this work, the effect of nitrogen doping in carbon inverse opals was studied. The atomic structure, thermal stability, chemical composition, optical and electrical properties are described in detail. We believe that these novel materials could be used for the fabrication of optoelectronic devices, sensors, adsorption filters, batteries, capacitors, etc.

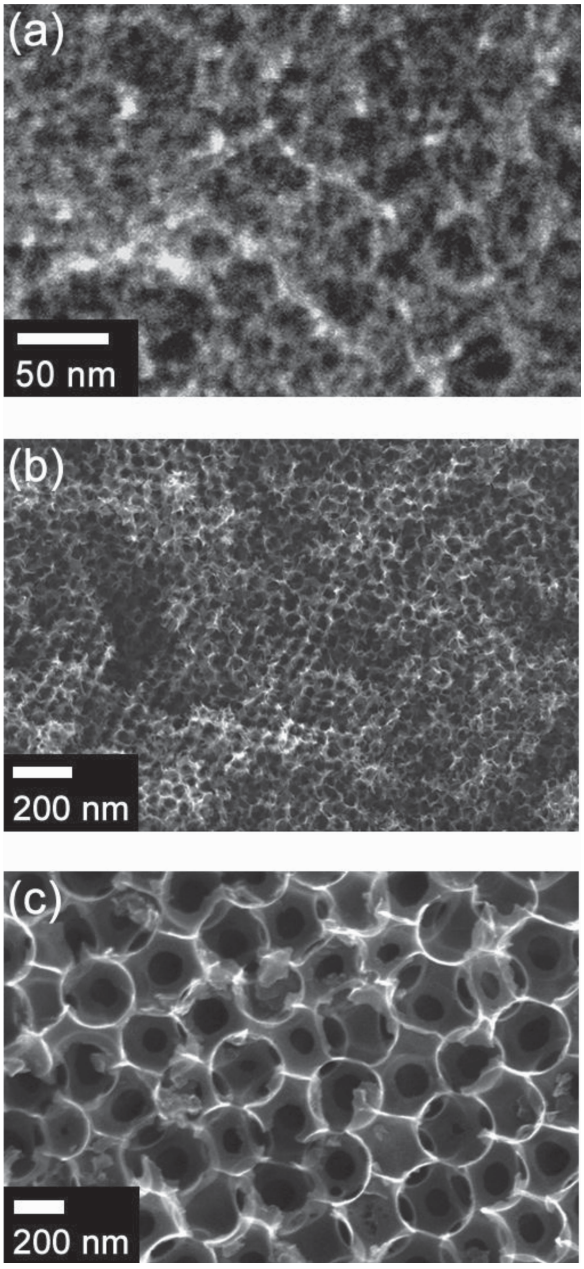

Figure 1. Scanning electron microscopy (SEM) images of carbon inverse opals using a) 10, b) 100, and c) 300 nm silica nanoparticle. Samples at different N content do not show any morphological changes.

2. Results and Discussion

SEM images of carbon inverse opal (CIO) doped with different nitrogen content and using 10, 100 and 300 nm silica particles show the pore arrays after the removal of the silica nanospheres from the opals (see **Figure 1**). It seems that the introduction of nitrogen does not inhibit the formation of uniform carbon walls within the inverse opals. For all inverted opals, pore sizes and distributions were obtained from SEM images by performing 100 independent measurements. The overall average of pore size was 9 ± 1 nm, 112 ± 1 nm, and 292 ± 6 nm, for CIO10, CIO100, and CIO300 samples. The walls of the pores appeared to be smooth and replicated the voids of the opal. We found that only for the 300 nm silica particles the pores appeared well ordered over large volumes, and exhibited an FCC arrangement caused by the original opal structure used to impregnate with carbon.

TEM images of the CIO reveal the arrays of the pores (**Figure 2**), and it is noteworthy that those obtained with the 300 nm silica particles exhibit an almost perfect order (Figure 2a,d). TEM images also indicate that CIO with smaller pore sizes are disordered (Figure 2a,c). It is also observed that inverse opals produced in the presence of nitrogen (CIO300-N3)

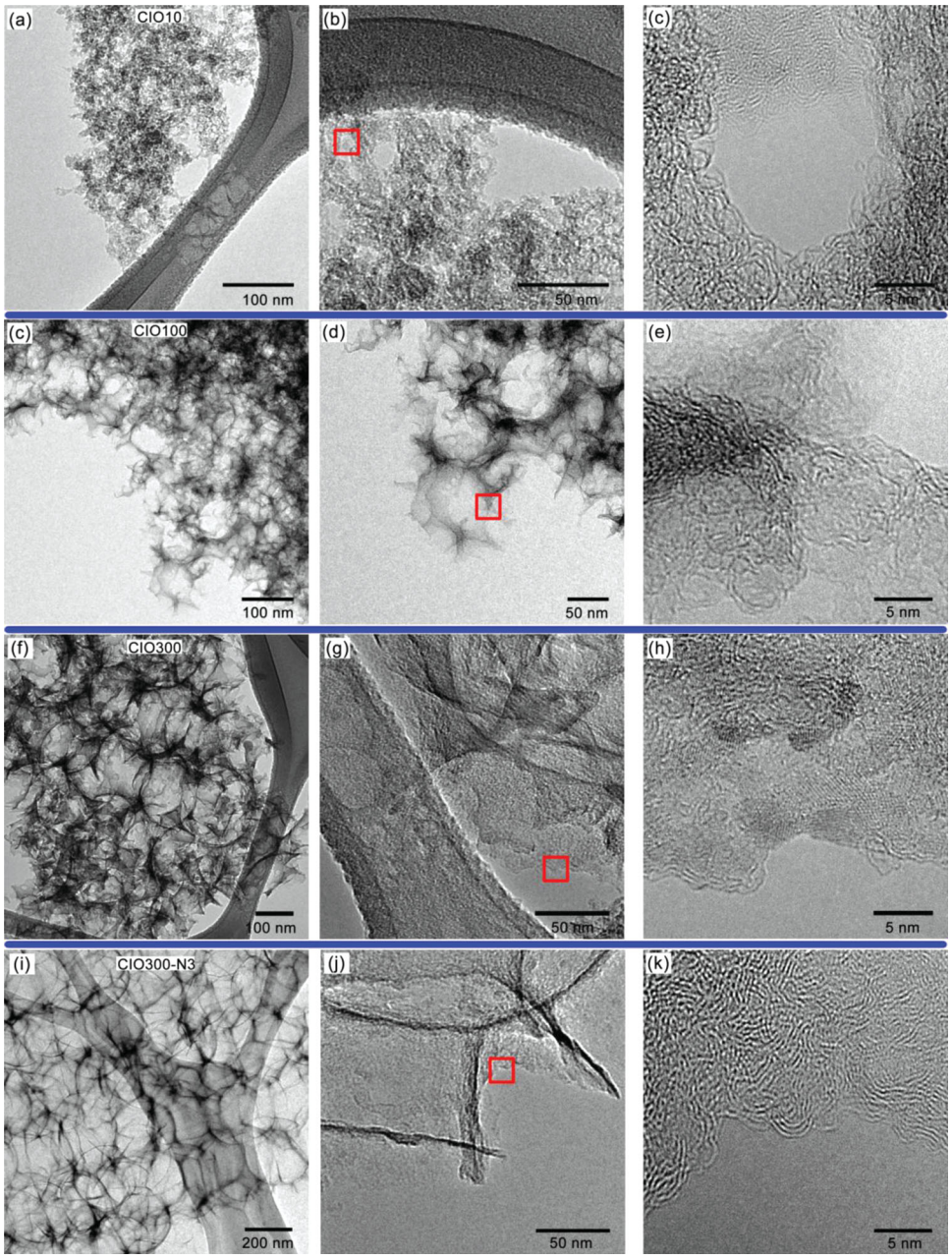

Figure 2. Transmission electron microscopy (TEM) images of carbon inverse opal a–c) 10, d–f)100, and g–i) 300 nm pore size. TEM images of i–k) carbon inverse opal doped with the highest content of nitrogen (N3). Left: low magnification TEM images show porous structure. Right: high magnification TEM images showing the structure of the carbon walls.

exhibit a periodic array of pores (Figure 2i–k) containing curled graphene-like layers (Figure 2k). Similar curled structures have been observed by Harris et al.[16] These authors concluded that the curled structures consist of fragments of different Schwarzites.[34]

Figure 3a shows the Raman spectra of CIO300 samples (undoped and N-doped with different pyrazine concentrations). The presence of an intense D-band at ≈1340 cm^{-1} indicates that the perfect hexagonal symmetry of sp^2 hybridized carbon is being broken by the introduction of defects, curvature and dopants within the CIO samples. The intensity values for I_D/I_G are plotted in Figure 3b for CIO10, CIO100, and CO300. We observe that CIO samples prepared with 10 and 100 nm silica particles exhibit similar tendency: I_D/I_G becomes smaller as the pyrazine/sucrose ratio increases, thus indicating a relative enhancement in the degree of crystallinity of the materials (Figure 3b). This suggests that pyrazine might be considered a crystallizing agent (e.g., more graphite-like structures) due to its aromatic structure.[15] However, when using 300 nm-size silica nanoparticles and high concentrations of pyrazine in

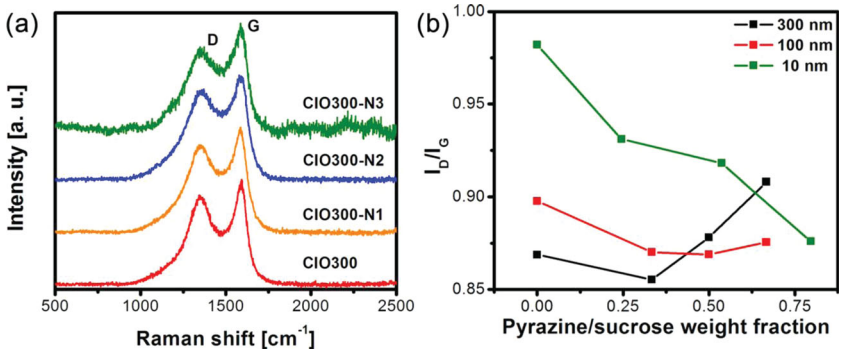

Figure 3. a) Raman spectroscopy of carbon inverse opal doped with Nitrogen at different concentrations of pyrazine using 300 nm. With 10 and 100 nm particles the shapes of the spectra are similar. b) Tendency of I_D/I_G ratio of carbon inverse opals doped with different concentrations of nitrogen and silica nanoparticle sizes (10, 100, and 300 nm).

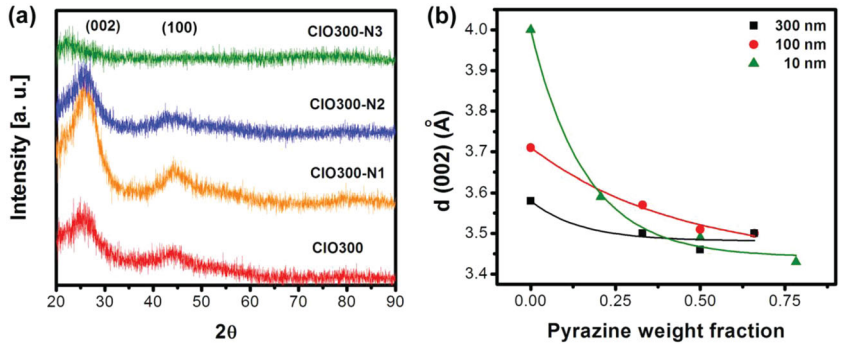

Figure 4. a) X-ray powder diffraction patterns of carbon inverse opals made with 300 nm size particles at different concentrations of pyrazine. With 10 and 100 nm particles the shapes of the diffraction patterns are similar. b) Interplanar distance of plane (002) of carbon inverse opals with different particle size and concentration of pyrazine.

the solution, the degree of crystallization of the N-doped CIO is reduced (Figure 3b). Furthermore, when the position of the D- and G- bands were analyzed, we found a clear upshift for the D peak when increasing the amount of pyrazine used for synthesis from ≈1344 cm^{-1} to ≈1358 cm^{-1} (see **Table 1**). This effect could be caused by the nitrogen doping and variations in the degree of crystallinity.[35,36] In addition, the G-band exhibits a downshift that can be associated to the introduction of structural defects, which in this case includes nitrogen doping (Table 1).[37]

Powder X-ray diffraction of all the samples showed reflections around 2θ = 26 and 44 degrees, corresponding to the (002) and (100) planes of graphite (**Figure 4**a,b), respectively. Similar patterns have been observed by Buiel et al.,[38] and the (002) peaks indicate the presence of several stacked graphene sheets within the CIO. We observed that smaller silica particles used in the synthesis of CIO resulted in larger interplanar distances.[39] For CIO300-NY, the graphitic order (e.g. number of stacked layers) decreases when the pyrazine content is increased until sample CIO300-N2, possibly due to the presence of nitrogen atoms that are responsible of breaking the hexagonal symmetry order of sp^2 hybridized carbon. Here, the minimum interlayer spacing varies from 3.58 Å to 3.46 Å. However for CIO10-NY and CIO100-NY, we noted that the interlayer spacing reaches a minimum at higher nitrogen concentrations (N3): varying from the undoped to the nitrogen doped samples from 3.99–3.43 Å and 3.70–3.49 Å, respectively. Therefore, pyrazine aids the formation of stacked graphite-like layers in our experiments.

When considering the classification of pyrolized carbon sources made by R. E. Franklin, a non-graphitizable carbon source contains both a small amount of hydrogen and a higher amount of oxygen in its molecular composition.[15] For the graphitizable carbon source, a high content of hydrogen and a small amount or null amount of oxygen takes place. In this context, sucrose is non-graphitizable and pyrazine (an aromatic molecule) is graphitizable. It is possible that due to the aromatic structure of pyrazine, CIO10 and CIO100 samples could be incorporating a higher concentration of pyrazine that results in more graphite-like material with a high degree of crystallinity (see Raman spectroscopy data). For CIO300, as the pyridine-type nitrogen increases, the corrugation of the layers augments and the degree of crystallinity decreases.[28]

X-ray photoelectron spectroscopy (XPS) was used to determine the chemical surface composition of the CIO300-NY materials, and also provided relevant information regarding the binding energies of carbon and nitrogen within the synthesized materials (see **Figure 5**). The carbon C 1s region for all samples reveal the presence of sp^2 and sp^3 binding energies (284.3 and 285.2 eV, respectively). For the C 1s signal, all the samples exhibited peaks assigned to C–O (286 eV), C=O (286.7), and O–C=O (287.5 eV).[40–43]

Table 1. Position of peaks (cm^{-1}) in the Raman spectra measured for the samples synthesized with conditions CIOX, CIOX-N1, CIOX-N2, and CIOX-N3, the letter "X" corresponds to the particle size used (10, 100, and 300 nm). Notice that the D peak upshifts with increasing pyrazine content.

D	CIOX	CIOX-N1	CIOX-N2	CIOX-N3
10 nm	1346	1344	1350	1353
100 nm	1342	1352	1358	1349
300 nm	1351	1355	1356	1358
G				
10 nm	1600	1594	1598	1590
100 nm	1583	1589	1590	1590
300 nm	1592	1586	1596	1585
I_D/I_G				
10 nm	0.973	0.931	0.917	0.876
100 nm	0.897	0.870	0.869	0.875
300 nm	0.869	0.855	0.878	0.908

Table 2. Elemental analysis obtained from XPS measurements for undoped and nitrogen doped carbon inverse opals made with 300 nm particles.

at%	CIO300	CIO300-N1	CIO300-N2	CIO300-N3
C	96.19	93.75	93.97	89.34
N	0.00	1.04	2.43	5.48
O	3.89	5.21	3.6	5.18

The nitrogen N 1s region indicates the presence of pyrrolic (or N atoms bonded to two carbon atoms contributing to the π–system with two p-electrons) located at binding energies of 401.5 eV, pyridinc nitrogen (or N atoms bonded to two carbon atoms atoms contributing to the π–system with one p-electrons) located at energies of 399.5 eV and quaternary nitrogen at 402.6 eV (or N atoms bonded to three carbon atoms in a substitutional manner).[41,43,44] The atomic concentrations obtained from the XPS analysis indicate that samples contain 1.05 at%, 2.43 at%, and 5.48 at% of nitrogen for CIO300-N1, CIO300-N2, and CIO300-N3, respectively (see **Table 2**).

We also performed surface area analysis by nitrogen absorption with Brunauer–Emmett–Teller (BET) theory of all the undoped and doped CIO synthesized using different amounts of pyrazine (**Figure 6**a). The highest surface area was obtained for pore sizes of 10 nm CIO10-N1 with a value of 1540 m^2 g^{-1}. For CIO10-NY and CIO100-NY samples, we found that the surface area tends to decrease when the concentration of pyrazine is increased; these results agree with the findings reported by other research groups.[9,45–47] However, for CIO300-N3 the surface area increases from 94 to 163 m^2 g^{-1} (**Table 3**). Therefore, and due to the large surface areas found, we believe that these CIO materials could serve as efficient gas sensor materials with novel catalytic activities. In addition, the presence of nitrogen in the CIO could make the materials more reactive.

From the thermogravimetric analysis (TGA) analysis in air, we observed the loss of the majority of the material. We believe that the residual non-burned material (5% by wt. to 10% by wt.) at the end of the TGA may come from the undisolved SiO_2 during the etching process (see crystalline domains in Figure 2h). It is clear that for samples exhibiting 10 and 300 nm pore sizes, the decompostion temperature increases when increasing the pyrazine content (Figure 6 b). However, CIO samples with 100 nm pore always tend to decrease the decomposition temperature when increasing the pyrazine content.

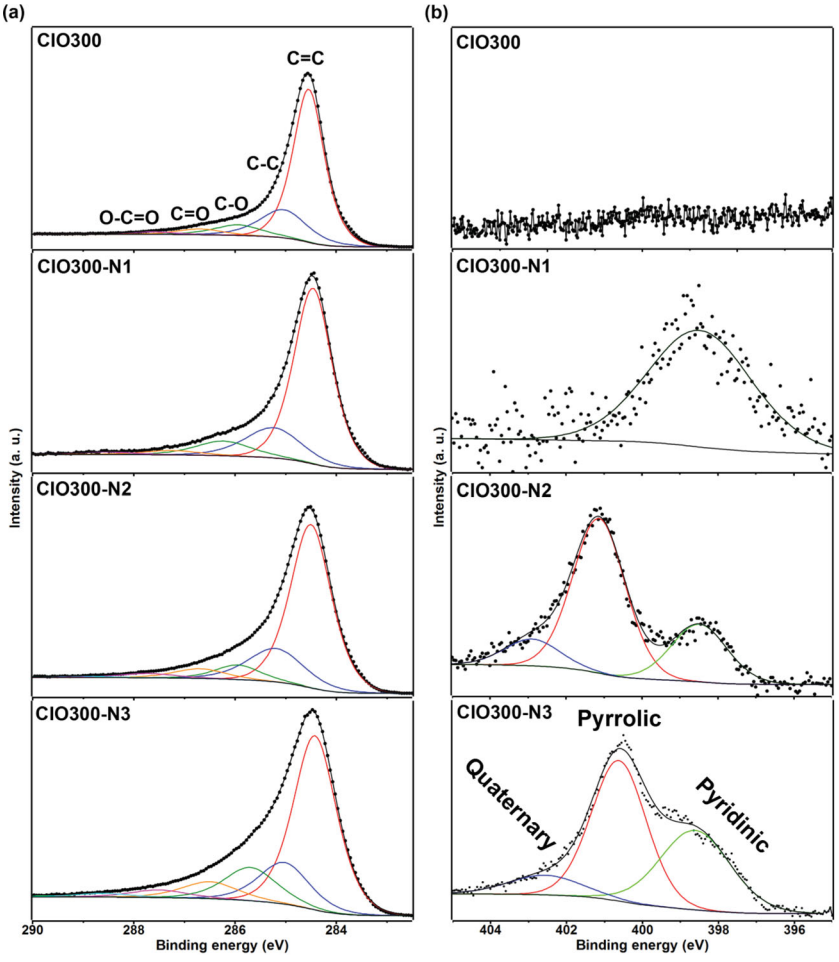

Figure 5. High resolution X-ray photoelectron spectra of carbon inverse opal (upper spectra) and nitrogen doped carbon inverse opal of a) C 1s and b) N 1s. It is clear that the undoped carbon inverse opal does not contain nitrogen.

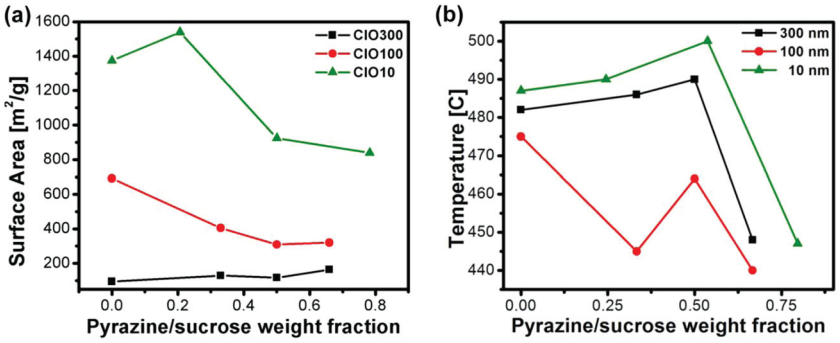

Figure 6. a) Surface area obtained by nitrogen absorption using BET and b) decomposition temperature for carbon inverse opal with 10, 100 and 300 nm pore size at different amounts of pyrazine used for synthesis.

UV-Vis reflection spectra were recorded for the different synthesized opals, doped and undoped obtained with the 300 nm silica particles (**Figure 7**a). Under a bright white light it is possible to observe the colors revealed by the UV-VIS spectra (Figure 7b–f). The pure opal shows a red reflected color (625 nm) that is also observed for the undoped carbon inverse opal (CIO300) at wavelengths of 609 nm. Interestingly, when we introduced pyrazine up to a 50% (CIO300-N2) the reflection shifts down to the blue region of the spectrum (466 nm); and for 33% of pyrazine (CIO300-N1), a peak appears at 568 nm. In addition, CIO300 and CIO300-N1 samples displayed secondary peaks located at 493 and 483 nm, respectively. Using 75% of pyrazine (CIO300-N3), the reflection peak downshifts to a green color (528 nm). From these results, it was confirmed that different concentrations of nitrogen within CIO could tune the optical properties significantly, similar to the reported CIO doped with K.[21]

Furthermore, after conducting four probe electrical measurements, we observed that all the samples behave as a semiconductor (**Figure 8**a) with an increase in the electrical conductivity by one order of magnitude from 2 S cm^{-1} (0.30 Ω cm) in CIO300 to 30 S cm^{-1} (0.02 Ω cm) in CIO300-N2. We applied the variable range hopping (VRH) theory to our data in order to understand better the electrical transport mechanism (Figure 8b).[48] The data was plotted as $Ln(\sigma(T)/\sigma(300))$ versus $T^{-1/2}$, $T^{-1/3}$, or $T^{-1/3}$ for Coulomb gap, 2-dimensional and 3-dimensional VRH, respectively (Figure SI-1, Supporting Information). A linear fit was applied for each plot and their corresponding coefficient of determination (R^2) was obtained (Table SI-1, Supporting Information). From the R^2 values we could determine that all the samples had a better fitting for 3-dimensional VRH (3D-VRH) for temperatures below 100 K, as observed for carbon networks by Govor et al.[49] This 3D-VRH indicated that the electrons are moving throughout the entire 3-dimensional structure of the CIOs. For all samples studied, the electrical conductivities and optical properties vary similarly (see Figure 8). For example, when the electrical conductivity is increased by one order of magnitude from 2 in CIO300 to 30 S cm^{-1} in CIO300-N2 (at room temperature) the reflection color varies from red to blue, and then CIO300-N3 has an decrease in conductivity and an optical shift to green. The changes of the dielectric constant and electrical properties upon nitrogen doping in amorphous carbon has been reported by Yu et al., and attributed to changes in the carbon hybridization caused by the nitrogen doping.[23] The variations among the optical properties and electrical resistivity suggest that the optical and electrical properties are effectively modified by the introduction of nitrogen species within the CIO materials.

From the characterization data, it also appears that the silica particle size and the content of pyrazine significantly altered the chemical and physical properties of the CIO samples.

Table 3. Measured surface area of CIO with different pore size at distinct pyrazine content for synthesis. These values were obtained with the Brunauer–Emmett–Teller (BET) theory.

	[m^2 g^{-1}]
CIO10	1374
CIO10-N1	1539
CIO10-N2	923
CIO10-N3	839
CIO100	691
CIO100-N1	405
CIO100-N2	309
CIO100-N3	320
CIO300	94
CIO300-N1	130
CIO300-N2	117
CIO300-N3	163

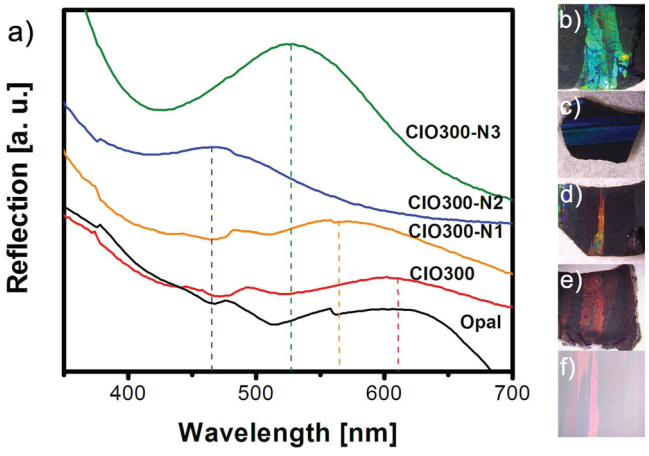

Figure 7. a) UV-VIS reflection spectra of carbon inverse opal with 300 nm particle at different pyrazine concentrations. b–f) Photograph of carbon inverse opal from CIO300-N3 to CIO300-N1, CIO and opal, respectively.

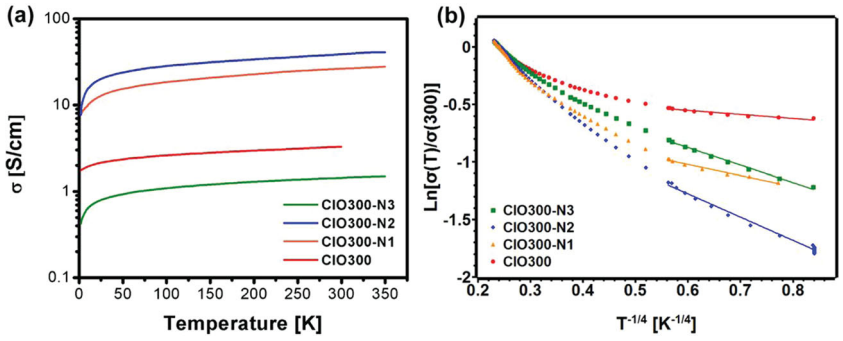

Figure 8. a) Conductivity vs temperature of nitrogen doped carbon inverse opal (made with 300 nm silica particles) at different contents of pyrazine, all samples present a semiconductor behavior. Marked reduction of resistivity is observed from 2 to 30 S/cm from CIO300 to CIO300-N2. b) 3-dimensional variable range hopping fitting for the before mentioned samples.

Overall, the CIO300 series exhibits the highest degree of crystallinity and the CIO10 series exhibits the lowest values, as observed by Raman spectroscopy and XRD data. The introduction of pyrazine varies the CIO properties distinctly according to the used silica particle size. For CIO100-NY and CIO10-NY the degree of crystallinity is enhanced, with a more significant effect when dealing with CIO10-NY samples. Here, it is possible that the introduction of nitrogen atoms from the thermolysis of pyrazine may favor the formation of well ordered stacked graphite-like layers as opposed to sucrose which provides more amorphous-like materials.[15] The small particle size may constrict the carbonization, aiding the formation of graphitic domains as observed in the fabrication of graphite films with polymers using a hot pressing furnace.[50] However, for CIO300 the graphitic stacking is not greatly affected and the content of defects is increased due to nitrogen doping.

3. Conclusion

The doping of CIO with nitrogen was studied systematically using different silica nanoparticle sizes and by varying the concentration of the nitrogen-carbon source when impregnating the silica. First of all, smaller size particles results in a less crystalline carbon material, and the (002) interplanar distance increases. However, with the introduction of pyrazine, the degree of crystallinity and the graphite-like stacking are improved. The use of a non-graphitizable and a graphitizable carbon sources together might be a route to control the chemical and physical properties of CIO. The chemical composition of all samples show changes in the oxidation resistance of the carbon surface due to nitrogen bonded with carbon (e.g., in a substituional and pyridinic configuration).

The optical properties of the materials were studied by UV-Vis spectroscopy, and the introduction of nitrogen within the CIO clearly varied the position of peaks, by lowering the wavelength depending on the content of pyrazine used in the CIO synthesis. The conductivity measurements exhibited an increase in the conductivity by one order of magnitude from 2 to 30 S cm^{-1} (at room temperature) when the pyrazine content was increased to 12.50% by wt.

This work demonstrates that it is indeed possible to control the chemical composition of the CIO by doping with nitrogen. Therefore, one could tune their optical and electrical properties. We believe this material may find appllications as optoelectronic materials, sensors, field emitters, biomaterials, 3-dimensional scaffolds and others.

Table 4. Carbon and nitrogen source solution concentrations, quantities are in% by wt., the letter "X" corresponds to the particle size used (X = 300, 100, and 10 nm).

	CIOX	CIOX-N1	CIOX-N2	CIOX-N3
Sucrose	25.00	16.67	12.50	8.33
Pyrazine	0.00	8.33	12.50	16.67
Sulphuric acid	2.58	4.17	6.25	8.33
Water	72.42	70.83	68.75	66.67

4. Experimental Section

Opals with 300 nm particles (101 surface plane), 100 and Ludox-SM30 (disordered opal with ≈10 nm particles) were held in a solution of sucrose ($C_{12}H_{22}O_{11}$), pyrazine ($C_4H_4N_2$) the source of nitrogen for doping, sulphuric acid (H_2SO_4) and destilled water (according to **Table 4**) at 80 °C during 6.5 h. Sucrose and sulphuric acid react thus leaving carbon and hydrated sulphuric acid in the medium. After the evaporation of water, the samples were held at 1000 °C during one hour in Ar atmosphere, this was followed by an HF (30% in water) treatment during one day so as to remove the silica nanoparticles. In this study, our samples were labeled as follows: CIOX-NY, in which CIO corresponds to carbon inverse opal, X is the size of the particle used in the synthesis with possible values of 300, 100, or 10 nm, and Y the pyrazine content (1 = 8.33% by wt., 2 = 12.50% by wt. and 3 = 16.67% by wt.) For example, CIO300-N2 would correspond to 300 nm silica particle size and pyrazine content of 12.50% by wt.

These samples were analyzed by scanning electron microscopy (SEM) (Zeiss-LEO Model 1530, Zeiss Supra 40 and XL 30 SFEG FEI operated between 10–20 kV), X-ray diffraction (XRD) (Difractometer D8 Advanced Bruker), Raman spectroscopy (Renishaw inVia Raman microscope, Ar laser 514.5 nm and Jobin Yvon LabRam HR Micro-Raman), UV-VIS spectroscopy (Perkin Elmer Lambda 900 UV-Vis/NIR Spectrophotometer) and resistivity measurements (between 2 K and 300 K) using a PPMS Quantum Design Device with a four probe configuration. Surface chemical analysis was performed by X-ray photoelectron spectroscopy (XPS) using an Axis-Ultra, Kratos, UK apparatus. The analysis of the XPS spectra was carried out using Casa XPS ver. 2.3.16 software.

Acknowledgements

The authors are grateful to D. Ramírez-González, H. Martínez-Gutiérrez, F. Tristán-López, S. M. Vega-Diaz, B. A. Rivera-Escoto, G. J. Labrada-Delgado, and K. Gómez-Serrato for technical assistance, and E. E. Gracia-Espino for valuable discussions. This work was supported in part by CONACYT-México grant 48300 (E.M.S.) and Doctoral Scholarship (A.M.G.). A.M.G. acknowledges support from the New Energy and Industrial Technology Development Organization (NEDO). M.T. thanks

JST-Japan for funding the Research Center for Exotic Nano Carbons, under the Japanese Regional Innovation Strategy Program by the Excellence. M.T. acknowledges the financial support from the MURI project awards Nos. FA9550–12–1–0035 and FA9550–12–1–0471.

Received: October 1, 2013
Revised: November 14, 2013
Published online: January 13, 2014

[1] D. Cao, P. Feng, J. Wu, *Nano Lett.* **2004**, *4*, 1489.
[2] J.-S. Yu, S. Kang, S. B. Yoon, G. Chai, *J. Am. Chem. Soc.* **2002**, *124*, 9382.
[3] S. Han, K. Sohn, T. Hyeon, *Chem. Mater.* **2000**, *12*, 3337.
[4] V. G. Gavalas, N. A. Chaniotakis, T. D. Gibson, *Biosens. Bioelectron.* **1998**, *13*, 1205.
[5] S. Sotiropoulou, V. Gavalas, V. Vamvakaki, N.A. Chaniotakis, *Biosens. Bioelectron.* **2003**, *18*, 211.
[6] D.-Y. Kang, S.-O. Kim, Y. J. Chae, J. K. Lee, J. H. Moon, *Langmuir* **2013**, *29*, 1192.
[7] Y. Isshiki, M. Nakamura, S. Tabata, K. Dokko, M. Watanabe, *Polym. Adv. Technol.* **2011**, *22*, 1254.
[8] C.-M. Yang, K. Kaneko, *Carbon* **2001**, *39*, 1075.
[9] J. Machnikowski, B. Grzyb, J. V. Weber, E. Frackowiak, J. N. Rouzaud, F. Beguin, *Electrochem. Acta* **2004**, *49*, 423.
[10] J. Lahaye, G. Nanse, A. Bagreev, V. Strelko, *Carbon* **1999**, *37*, 585.
[11] A. A. Zakhidov, R. H. Baughman, Z. Iqbal, C. Cui, I. Khayrullin, S. O. Dantas, J. Marti, V. G. Ralchenko, *Science* **1998**, *282*, 897.
[12] H. Bu, J. Rong, Z. Yang, *Rapid Commun.* **2002**, *23*, 460.
[13] M. B. Shiflett, H. C. Foley, *Carbon* **2001**, *39*, 1421.
[14] R. Ryoo, S. H. Joo, S. Jun, *J. Phys. Chem. B.* **1999**, *103*, 7743.
[15] R. E. Franklin, *Proc. R. Soc. London Series A, Math. Phys. Sci.* **1951**, *209*, 196.
[16] P. J. F. Harris, A. Burian, S. Duber, *Phil. Mag. Lett.* **2000**, *80*, 381.
[17] P. J. F. Harris, *Crit. Rev. Sol. State Mater. Sc.* **2005**, *30*, 235.
[18] Y.-J. Lee, P. V. Braun, *Adv. Mater.* **2003**, *15*, 563.
[19] H. Takeda, K. Yoshino, *J. Appl. Phys.* **2002**, *92*, 5658.
[20] C. I. Aguirre, E. Reguera, A. Stein, *Adv. Funct. Mater* **2010**, *20*, 2565.
[21] H. Kajii, Y. Kawagishi, H. Take, K. Yoshino, A. A. Zakhidov, R. H. Baughman, *J. Appl. Phys.* **2000**, *88*, 758.
[22] Z. Y. Chen, J. P. Zhao, Y. H. Yu, X. Wang, S. Q. Yang, T. S. Shi, X. H. Liu, *Mater. Lett.* **1997**, *33*, 85.
[23] Y. H. Yu, Z. Y. Chen, E. Z. Luo, W. Y. Cheung, J. P. Zhao, X. Wang, J. B. Xu, S. P. Wong, I. H. Wilson, *J. App. Phys.* **2000**, *87*, 2874.
[24] X. Wang, P. J. Martin, *Appl. Phys. Lett.* **1996**, *68*, 1177.
[25] R. A. Sidik, A. B. Anderson, N. P. Subramanian, S. P. Kumaraguru, B. N. Popov, *J. Phys. Chem. B* **2006**, *110*, 1787.
[26] P. H. Chang, M. M. Labes. *Chem. Mater.* **1989**, *1*, 523.
[27] R. Czerw, M. Terrones, J.-C. Charlier, X. Blase, B. Foley, R. Kamalakaran, N. Grobert, H. Terrones, D. Tekleab, P. M. Ajayan, W. Blau, M. Rühle, D. L. Carroll, *Nano Lett.* **2001**, *1*, 457.
[28] M. Terrones, P. M. Ajayan, F. Banhart, X. Blase, D. L. Carroll, J. C. Charlier, R. Czerw, B. Foley, N. Grobert, R. Kamalakaran, P. Kohler-Redlich, M. Rühle, T. Seeger, H. Terrones, *Appl. Phys. A* **2002**, *74*, 355.
[29] R. Lv, Q. Li, A. R. Botello-Méndez, T. Hayashi, B. Wang, A. Berkdemir, Q. Hao, A. L. Elías, R. Cruz-Silva, H. R. Gutiérrez, Y. Ahm Kim, H. Muramatsu, J. Zhu, M. Endo, H. Terrones, J.-C. Charlier, M. Pan, M. Terrones, *Sci. Rep.* **2012**, *2*, 586.
[30] A. L. Elías, J. C. Carrero-Sánchez, H. Terrones, M. Endo, J. P. Laclette, M. Terrones. *Small* **2007**, *3*, 1723.
[31] S. Peng, K. Cho, *Nano Lett.* **2003**, *3*, 513.
[32] F. Villalpando-Pérez, A. H. Romero, E. Muñoz-Sandoval, L. M. Martínez, H. Terrones, M. Terrones, *Chem. Phys. Lett.* **2004**, *386*, 137.
[33] J. G. Lee, S. P. Lee, *Sens. Actuators B* **2005**, *108*, 450.
[34] H. Terrones, M. Terrones, *New J. Phys* **2003**, *126*, 1.
[35] L. G. Bulusheva, A. V. Okotrub, I. A. Kinloch, I. P. Asanov, A. G. Kurenya, A. G. Kudashov, X. Chen, H. Song, *Phys. Stat. Sol. B* **2008**, *245*, 1971.
[36] R. O. Dillon, John A. Woollam, V. Katkanant, *Phys. Rev. B.* **1984**, 3482.
[37] A. C. Ferrari, J. Robertson, *Phys. Rev. B* **2000**, *61*, 14096.
[38] E. R. Buiel, A. E. George, J. R. Dahn, *Carbon* **1999**, *37*, 1399.
[39] H. Take, T. Matsumoto, S. Hiwatashi, T. Nakayama, K. Nihara, K. Yoshino, *Jpn. J. Appl. Phys.* **2004**, *43*, 4453.
[40] S. Talapatra, P. G. Ganesan, T. Kim, R. Vajtai, M. Huang, M. Shima, G. Ramanath, D. Srivastava, S. C. Deevi, P. M. Ajayan, *Phys. Rev. Lett.* **2005**, *95*, 097201.
[41] S. Maldonado, S. Morin, K. J. Stevenson, *Carbon* **2006**, *44*, 1429.
[42] M. Tabbal, P. Mérel, S. Moisa, M. Chaker, A. Ricard, M. Moisan, *Appl. Phys. Lett.* **1996**, *69*, 1698.
[43] Z. Yue, K. R. Benak, J. Wang, C. L. Mangun, J. Economy, *J. Mater. Chem.* **2005**, *15*, 3142.
[44] T. Sharifi, G. Hu, X. Jia, T. Wågberg, *ACS Nano* **2012**, *6*, 8904.
[45] M.-C. Huang, H. Teng, *Carbon* **2003**, *41*, 951
[46] E. Raymundo-Piñero, D. Cazorla-Amorós, A. Linares-Solano, *Carbon* **2003**, *41*, 1925.
[47] P.-X. Hou, H. Orikasa, T. Yamazaki, K. Matsuoka, A. Tomita, N. Setoyama, Y. Fukushima, T. Kyotani, *Chem. Mater.* **2005**, *17*, 5187.
[48] B. I. Shklovskii, A. L. Efros, Electonic Properties of Doped Semiconductors, In: Spring Series In Solid-State Sciences 45, Springer, New York **1984**.
[49] L. V. Govor, M. Goldbach, I. A. Bashmakov, I. B. Butylina, *J. Parisi. Phys. Rev. B* **2000**, *62*, 2201.
[50] Y. Kaburagi, Y. Hishiyama, *Carbon* **1995**, *33*, 773.